Selenium quantum dots: Preparation, structure, and properties

Cite as: Appl. Phys. Lett. **110**, 053104 (2017); https://doi.org/10.1063/1.4975358
Submitted: 20 September 2016 . Accepted: 19 January 2017 . Published Online: 31 January 2017

Fuli Qian, Xueming Li, Libin Tang, Sin Ki Lai, Chaoyu Lu, and Shu Ping Lau

Selenium quantum dots: Preparation, structure, and properties

Fuli Qian,[1] Xueming Li,[1,a)] Libin Tang,[2,b)] Sin Ki Lai,[3] Chaoyu Lu,[1] and Shu Ping Lau[3]
[1]*Solar Energy Research Institute, Yunnan Normal University, Kunming 650500, People's Republic of China*
[2]*Kunming Institute of Physics, Kunming 650223, People's Republic of China*
[3]*Department of Applied Physics, The Hong Kong Polytechnic University, Hong Kong, People's Republic of China*

(Received 20 September 2016; accepted 19 January 2017; published online 31 January 2017)

An interesting class of low-dimensional nanomaterials, namely, selenium quantum dots (SeQDs), which are composed of nano-sized selenium particles, is reported in this study. The SeQDs possess a hexagonal crystal structure. They can be synthesized in large quantity by ultrasound liquid-phase exfoliation using $NbSe_2$ powders as the source material and N-Methyl-2-pyrrolidone (NMP) as the dispersant. During sonication, the Nb-Se bonds dissociate; the SeQDs are formed, while niobium is separated by centrifugation. The SeQDs have a narrow diameter distribution from 1.9 to 4.6 nm and can be dispersed with high stability in NMP without the need for passivating agents. They exhibit photoluminescence properties that are expected to find useful applications in bioimaging, optoelectronics, as well as nanocomposites. *Published by AIP Publishing.* [http://dx.doi.org/10.1063/1.4975358]

Following the discovery of graphene in 2004,[1] two-dimensional (2*D*) materials have become an important research field in the past decade. They find useful applications in batteries where materials with nanoscale thicknesses stacked into electrodes can allow enhancement in ion-insertions[2] and in electronics where transistors made from 2*D* materials have shown excellent on/off ratios and mobilities, which may open up new avenues for the down-scaling of transistors.[3,4] Low-dimensional materials, especially quantum dots (QDs), have triggered many new research hot spots in various fields of materials science. The QDs are physically confined in all three dimensions, which results in discrete energy levels[5] and an increase in band gap such that QDs commonly have different fluorescent properties from their bulk counterpart. The fluorescent properties can be further tuned by changing their sizes,[6] doping with hetero-atoms,[7] or surface ligand engineering,[8] which has also become an active research area. Fluorescent quantum dots, like graphene quantum dots, with size typically less than 10 nm, had also found promising application in bioimaging where the nano-sized bio-compatible dots can diffuse into cells for feature imaging under a microscope.[9–13]

With the success of graphene, layered materials, especially two-dimensional materials, have attracted intensive attention. Research efforts mainly focused on group IV elements like silicene,[14] germanene,[15] and stanine.[16] In particular, silicene showed potential to integrate with existing silicon semiconductor electronics.[17] The promising properties of these "carbon-group" materials have provided motivation to investigate other low-dimensional materials.

Selenium nanoparticles[18–21] with diameters of ca. 15–200 nm have been prepared by various methods, such as γ-irradiation,[18] reducing selenious acid,[19] and chemical reduction methods.[20] The structural and absorption properties of selenium nanoparticles have been investigated.

Selenium quantum dots (SeQDs) have been prepared by laser irradiation of water suspended Se nanoparticles; it is found that the size and optical properties of SeQDs are affected by laser irradiation time. Phase conversion has also been found by the laser irradiation method.[22] A simple method to prepare good crystalline SeQDs with narrow size distribution and low defects is desired. In this study, nano-sized Se dots with good crystallinity, namely, selenium quantum dots, with diameters below 10 nm, have been synthesized and the optical properties of which were investigated.

About 0.5 g of niobium(IV) selenide ($NbSe_2$) powders (Alfa Aesar) was mechanically ground into fine powders, which was then added to 50 ml N-Methyl-2-pyrrolidone (NMP) (Aladdin) and was sonicated continuously for 4 h in a high power (500 W) ultrasound bath. During sonication, the $NbSe_2$ layers, which are bounded by weak van der Waals force, exfoliated due to the intercalation of NMP into the layers under the influence of ultrasound. The synthesis mechanism of SeQDs would be further discussed in the below paragraph. The dispersant was then centrifuged at 2000 rpm for 25 min, and the supernatant was collected to give the SeQDs/NMP solution.

Transmission electron microscopy (TEM) was performed on a JEM-2100 electron microscope operating at 200 kV. The TEM samples were prepared by drop-casting SeQDs/NMP solution onto a carbon-coated copper grid and then dried naturally. The morphology and height of SeQDs were characterized by atomic force microscopy (AFM, SPA-400). The chemical bonding was analyzed by x-ray photoelectron microscopy (XPS, PHI Versa probe II) using 50 W Al Kα radiation. X-ray diffraction (XRD) was carried out with a Rigaku-TTR III X-ray diffractometer (Cu Kα radiation, $\lambda = 1.54056$ Å) operating at 45 kV and 200 mA, with a scan range of 2θ from 5° to 90°. The Fourier Transform infrared (FTIR) spectrum was measured by a Thermo Nicolet Avatar 360 spectrometer using the KBr pellet technique. The UV-visible absorption was measured by a UV-Vis (Specord 200) spectrometer using deionized water as the reference. The fluorescence spectra were obtained from a Hitachi F-7000 fluorescence spectrometer. Raman spectra were acquired from a Renishaw in Via confocal Raman spectrometer with a 514.5 nm laser. The PL Quantum yield (QY) of the SeQDs was calculated by using quinine (QY = 0.54 in

a)E-mail: lxmscience@163.com
b)E-mail: scitang@163.com

24.9% ethanol) as the reference and was measured according to the following formula:[23,24]

$$Q_s = Q_r \times (I_s/I_r) \times (A_r/A_s) \times (n_s/n_r)^2, \quad (1)$$

where subscript "*s*" refers to the QY of the sample and subscript "*r*" refers to the reference. Q is the PL quantum yield; I is the emission peak area of fluorescence; A is the absorbance under specific excitation wavelength, and n is the refractive index. In sample preparation by FTIR spectroscopy, scanning electron microscope (SEM), and UV-vis measurements, the SeQD solid was obtained by heating the SeQDs/NMP solution to 80 °C.

Fig. 1(a) shows the TEM image of the SeQDs. The SeQDs have a spherical shape and disperse randomly on the grid without aggregation. The size distribution of the SeQDs is analyzed and shown in Fig. 1(b). Gaussian distribution was used to fit the data, from which the average diameter of the SeQDs was evaluated to be 2.95 nm, and the full-width-at-half-maximum (FWHM) of the distribution is 1.2 nm. To investigate the crystallinity of the SeQDs, high resolution TEM (HR-TEM) was carried out. Fig. 1(c) shows two SeQDs with diameters 2.7 nm and 3 nm, where lattice fringes of the SeQDs can be clearly identified, indicating good crystallinity of the SeQDs. Fast Fourier transform (FFT) performed on the 3 nm-SeQD in Fig. 1(c) is displayed in the inset of Fig. 1(d), which verified that the SeQDs have a hexagonal crystal structure, the same as the bulk Se crystal and also graphene. As a result, the SeQDs are classified as a low-dimensional nanomaterial. A magnified image of the 2.7 nm-SeQD is shown in Fig. 1(e), which reveals that the SeQDs are comprised of crystalline lattice planes. A line section along the red line is shown in Fig. 1(f). The distance between lattice fringes is 0.23 nm and is equidistant among each other.

Energy dispersive X-ray spectroscopy (EDS) analysis was carried out in an SEM. The corresponding result provided in Fig. 1(g) indicates that the atomic ratio of Se/O/C/N was given by 32/5/57/6, where the C, O, and N contents can be attributed to the NMP solvent.

Fig. 1(h) shows the XRD pattern of SeQDs. A number of peaks that correspond to the (100), (101), (102), (201), (112), and (103) lattice planes of the SeQDs can be identified, which are in excellent agreement with the XRD pattern of the Se single crystal (JCPDS#06-0362). Among the peaks, the (101) peak is the most prominent, which corresponds to a *d*-spacing of 0.31 nm. The (102) peak corresponds to a *d*-spacing of 0.21 nm, which agrees well with the lattice spacing obtained from TEM.

AFM was employed to further probe the height of SeQDs as presented in Fig. 2(a). The large bright dots with heights 13–30 nm are originated from the aggregated SeQDs as a consequence of the interaction between the high surface energy SeQDs and the hydrophobic silicon substrate. The SeQDs were attracted together to reduce the surface energy. Four individual SeQDs that can be observed are labelled as A, B, C, and D. Their heights are 3.59 nm, 2.86 nm, 2.55 nm, and 2.93 nm, respectively, as shown in Fig. 2(b). The average height is 2.98 nm, which is consistent with the average diameter given by TEM. The Raman spectrum of SeQDs is shown in Fig. 2(c). The Raman peak associates with Se can be identified at 236.2 cm^{-1}.[25]

To have a deeper understanding of the elemental composition and chemical bonding in the SeQDs, FTIR was carried out. The FTIR spectrum of the SeQDs is shown in Fig. 2(d). The peak at ~493.7 cm^{-1} is attributed to the Se-Se vibration. Other Se-related bonds are identified at C-Se (611.8 cm^{-1}). Based on the analysis of TEM, EDS, and FTIR, it can be concluded that the SeQDs have been synthesized.

To explain the formation mechanism of the SeQDs, characterizations were further carried out on the sediments collected from the centrifuged products. The EDS analysis

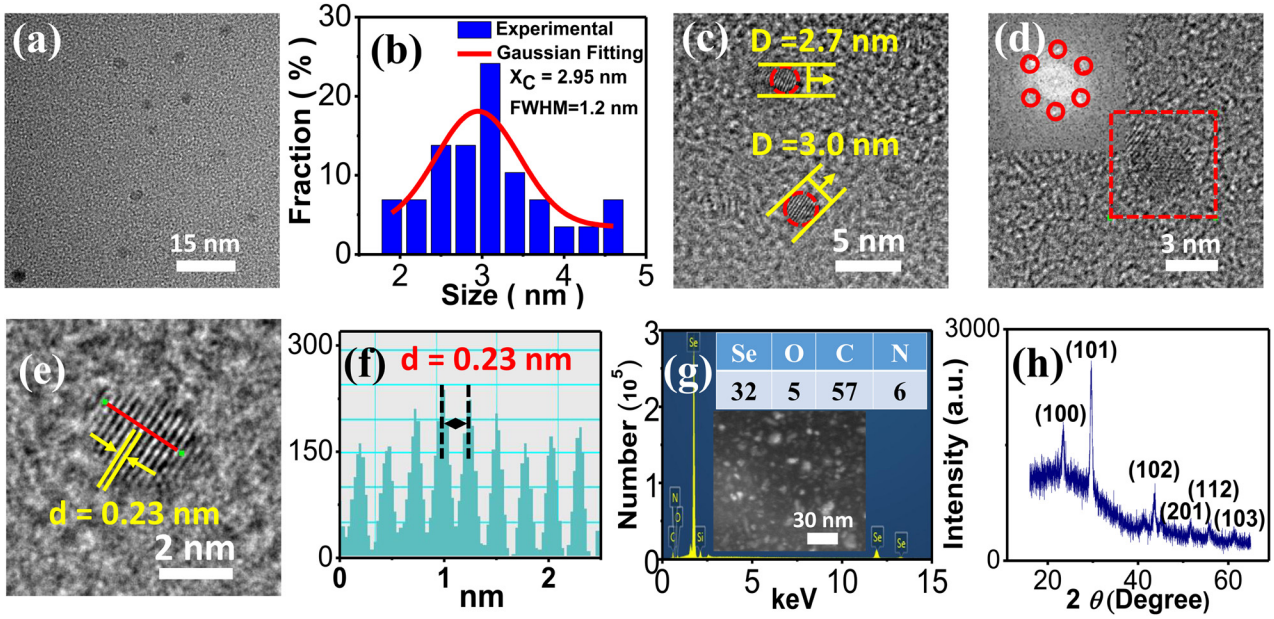

FIG. 1. Structural characterization of the SeQDs. (a) TEM image of the SeQDs. (b) The size distribution of the SeQDs. The red line is the Gaussian fitting. (c)–(e) The HR-TEM images of the SeQDs. Inset of (d): The FFT image of a selected area (red square). (f) The line section of the diffraction fringes in (e). (g) The EDS analysis of the SeQDs. The atomic ratio of Se/O/C/N is 32/5/57/6. (h) XRD pattern of the SeQDs.

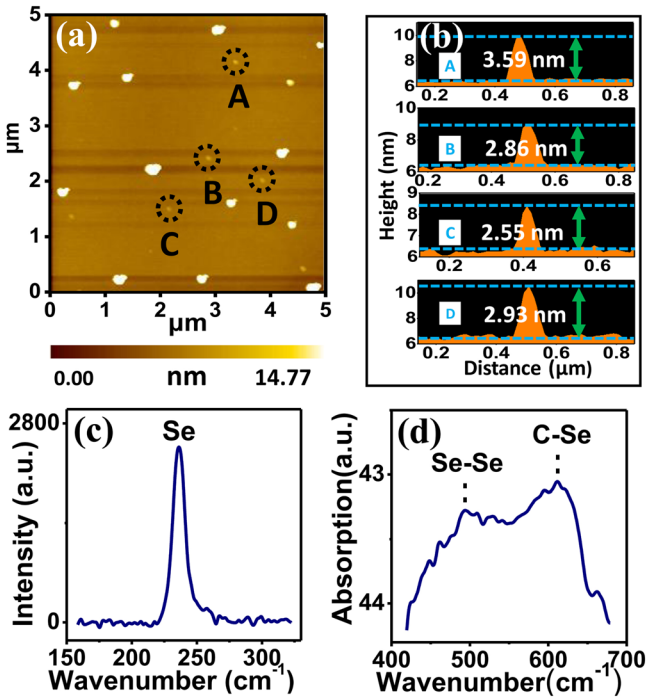

FIG. 2. (a) and (b) The AFM images of the SeQDs. (c) The Raman spectrum of the SeQDs drop-cast on the Si substrate. (d) The FTIR spectrum of the SeQDs.

of the sediments is shown in Fig. S1 in the supplementary material. It can be seen that the sediments contain a significant proportion of niobium, which is in contrast with the supernatant where nearly no niobium can be detected (see Fig. 1(g)). The XRD pattern of the sediments is shown in the supplementary material. Apart from the XRD peaks of $NbSe_2$, which were indicated by blue arrows, the peaks appeared at $2\theta = 38.5°$ and 55.6° are attributed to the (110) and (200) lattice planes of niobium, while the peaks at $2\theta = 45.3°$, 51.7°, and 54.8° are attributed to the (200), (201), and (220) planes of selenium. This provides evidence that there was a dissociation of Nb-Se bonds. Therefore, it can be deduced that the niobium detected in the sediments in the EDS measurement can be assigned to un-exfoliated $NbSe_2$ as well as niobium that results from the dissociation of Nb-Se bonds. Niobium settles at the bottom after centrifugation due to its higher density ($\rho_{Se} = 4.81\ g/cm^3$; $\rho_{Nb} = 8.57\ g/cm^3$). With the above information, together with the knowledge that the temperature required for thermal decomposition of $NbSe_2$ is higher than 900 °C, which is much higher than the condition employed in this experiment, and that the $NbSe_2$ does not react with NMP,[26] the formation mechanism of SeQDs can be concluded as follows: Under the effect of ultrasound, NMP intercalates into the layered structure of $NbSe_2$. It leads to the exfoliation of the atomic layers and dissociation of the Nb-Se bonds at the same time. Selenium arranges into the quantum dot size and dispersed in the solution. By carrying out centrifugation to separate different phases in the mixture, niobium that is denser precipitates to the bottom, and the purified SeQD solution is obtained in the supernatant.

The UV-vis spectrum of SeQDs is shown in Fig. 3(a). The SeQD solid was re-dispersed in DI water for measuring the UV-vis spectrum. The SeQDs exhibit an obvious absorption peak at 288 nm,[22] which becomes more recognizable as the SeQD solution becomes more concentrated. It absorbs strongly throughout the UV region from 200 nm to 400 nm. The PL spectra of the SeQD solution are shown in Fig. 3(b). As the excitation wavelength was changed to longer wavelength, the emission peak gradually red-shifted. This shows that SeQDs exhibit excitation wavelength dependent PL, which would be investigated in detail in the following section. Fig. 3(c) shows the photoluminescence excitation (PLE) spectra of the SeQDs. When the emission wavelength observed was at longer wavelength, the excitation wavelength that gives the maximum PL intensity at that emission wavelength also red-shifted, which is as expected and also consistent with Fig. 3(b), after having observed the excitation-dependent PL.

To investigate λ_{ex}-dependent PL and λ_{em}-dependent PLE of the SeQDs, the PL and PLE spectra are normalized as shown in Figs. 4(a) and 4(b), respectively. It can be clearly seen in Fig. 4(a) that as the excitation wavelengths are varied from 300 to 440 nm, in 20 nm interval, the PL peak position also red-shifted, by ~100 nm, from 408 to 509 nm. This property is also observed in graphene quantum dots.[27–30] In Fig. 4(b), as the emission wavelength under investigation was varied from 380 to 560 nm, in 20 nm interval, the excitation wavelength that gives the maximum emission also red-shifted from 337 to 432 nm. Lastly, the PL

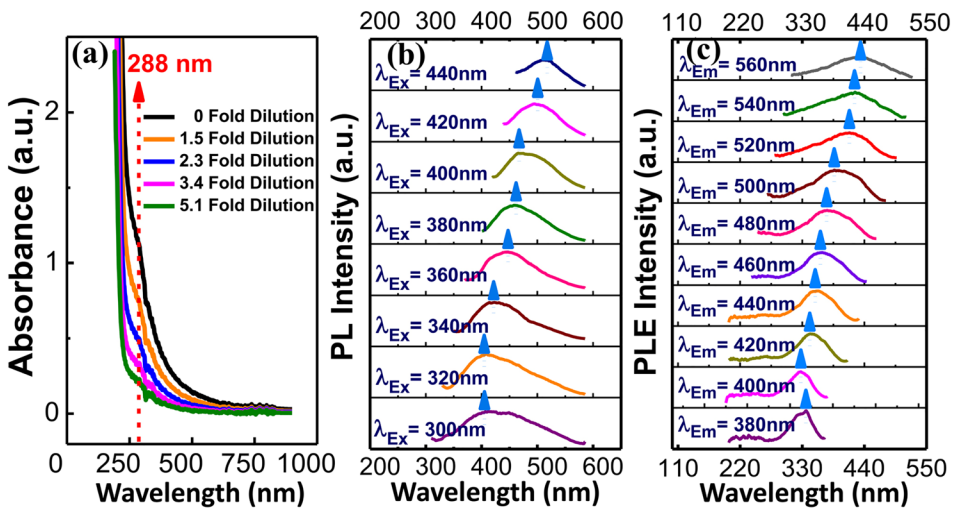

FIG. 3. (a) The UV-vis absorption spectrum of the SeQDs dispersed in deionized water with different dilution folds. (b) The PL emission spectra of the SeQD solution excited by wavelengths ranging from 300 nm to 440 nm, with 20 nm interval. (c) The PLE spectra of the SeQDs recorded as a function of emission wavelength ranging from 380 nm to 560 nm, with 20 nm interval.

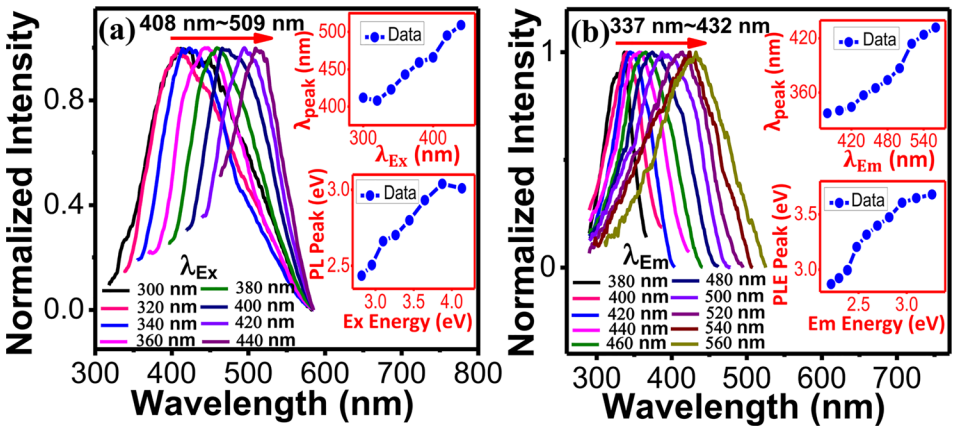

FIG. 4. (a) Normalized PL spectra of the SeQDs and (b) normalized PLE spectra of the SeQDs. Upper inset in (a): the linear relationship between the peak emission wavelength (λ_{peak}) and excitation wavelength (λ_{ex}), respectively. Upper inset in (b): the dependence of the PLE peak wavelength on the emission wavelength. Lower insets in (a) and (b) are presented with unit in energy (eV).

quantum yield (QY) of the SeQDs has been measured using Quinine (QY = 54%) as the reference with an emission wavelength of 288 nm. The QY of SeQDs was calculated to be ~22.7%, which is higher than that of graphene quantum dots with reported QY values ranging from 6% to 12%.[31,32] This reveals that SeQDs can be potentially a more powerful fluorescent probe than graphene quantum dots.

An interesting low-dimensional nanomaterial, namely, SeQD is synthesized using $NbSe_2$ powders and NMP mixture with high power sonication. The SeQDs have an average diameter of ~3 nm and a narrow size distribution. The SeQDs form stable dispersion in NMP with no sign of aggregation, and no passivating agent is required. The SeQDs show excellent fluorescent properties. Intensive blue PL was observed from the SeQDs under UV excitation. Excitation-wavelength-dependent PL was also observed from the SeQDs. The SeQDs gave a high PL quantum yield of 22.7%, which outperforms that of graphene quantum dots. Based on the excellent PL properties of the SeQDs uncovered in this work, the SeQDs are also expected to find useful applications as fluorescent probes and in optoelectronics.

See supplementary material for the EDS and XRD measurements on the sediments of the centrifuged product of the SeQDs/NMP mixture after ultrasound treatment (supplementary Figure S1).

This work was supported by the National Natural Science Foundation of China (Nos. 61106098 and 51462037) and the Key Project of Applied Basic Research of Yunnan Province, China (No. 2012FA003).

[1]K. S. Novoselov, A. K. Geim, S. V. Morozov, D. Jiang, Y. Zhang, S. V. Dubonos, I. V. Grigorieva, and A. A. Firsov, Science **306**, 666 (2004).
[2]P. R. Bueno, E. R. Leite, T. R. Giraldi, L. O. S. Bulhões, and E. Longo, J. Phys. Chem. B **107**, 8878 (2003).
[3]Z. Sun, Y. Zheng, J. Yao, E. Beitler, Y. Zhu, and J. M. Tour, Nature **468**, 549 (2010).
[4]L. Tao, E. Cinquanta, D. Chiappe, C. Grazianetti, M. Fanciulli, M. Dubey, A. Molle, and D. Akinwande, Nat. Nanotechnol. **10**, 227 (2015).
[5]H. Schoeller, *Transport Theory of Interacting Quantum Dots* (Springer, Netherlands, 1997).
[6]H. Kalita, J. Mohapatra, L. Pradhan, A. Mitra, D. Bahadurc, and M. Aslam, RSC Adv. **6**, 23518 (2016).
[7]F. Qian, X. Li, L. Tang, S. K. Lai, C. Lu, and P. L. Shu, AIP Adv. **6**, 075116 (2016).
[8]M. Mcdowell, A. E. Wright, and N. I. Hammer, Materials **3**, 614 (2010).
[9]S. Zhu, J. Zhang, C. Qiao, S. Tang, Y. Li, W. Yuan, B. Li, L. Tian, F. Liu, R. Hu, H. Gao, H. Wei, H. Zhang, H. Sun, and B. Yang, Chem. Commun. **47**, 6858 (2011).
[10]X. Michalet, F. F. Pinaud, L. A. Bentolila, J. M. Tsay, S. Doose, J. J. Li, G. Sundaresan, A. M. Wu, S. S. Gambhir, and S. Weiss, Science **307**, 538 (2005).
[11]Y. Zhang, Y. Li, and X. P. Yan, Small **5**, 185 (2009).
[12]Y. He, Y. Zhong, Y. Su, Y. Lu, Z. Jiang, F. Peng, T. Xu, S. Su, Q. Huang, C. Fan, and S. T. Lee, Angew. Chem., Int. Edit. **50**, 5695 (2011).
[13]B. A. Kairdolf, A. M. Smith, T. H. Stokes, M. D. Wang, A. N. Young, and S. Nie, Annu. Rev. Anal. Chem. **6**, 143 (2013).
[14]P. Vogt, P. De Padova, C. Quaresima, J. Avila, E. Frantzeskakis, M. C. Asensio, A. Resta, B. Ealet, and G. Le Lay, Phys. Rev. Lett. **108**, 155501 (2012).
[15]M. E. Dávila, L. Xian, S. Cahangirov, A. Rubio, and G. L. Lay, New J. Phys. **16**, 095002 (2014).
[16]F. F. Zhu, W. J. Chen, Y. Xu, C. L. Gao, D. D. Guan, C. H. Liu, D. Qian, S. C. Zhang, and J. F. Jia, Nat. Mater. **14**, 1020 (2015).
[17]S. Balendhran, S. Walia, H. Nili, S. Sriram, and M. Bhaskaran, Small **11**, 640 (2015).
[18]Y. Zhu, Y. Qian, H. Huang, and M. Zhang, Mater. Lett. **28**, 119 (1996).
[19]S. Y. Zhang, J. Zhang, H. Y. Wang, and H. Y. Chen, Mater. Lett. **58**, 2590 (2004).
[20]Z. H. Lin and C. R. C. Wang, Mater. Chem. Phys. **92**, 591 (2005).
[21]S. Sinha, S. K. Chatterjee, J. Ghosh, and A. K. Meikap, J. Appl. Phys. **113**, 123704 (2013).
[22]S. C. Singh, S. K. Mishra, R. K. Srivastava, and R. Gopal, J. Phys. Chem. C **114**, 17374 (2010).
[23]B. Song, C. D. B. Vandevyver, A. S. Chauvin, and J. C. G. Bünzli, Org. Biomol. Chem. **6**, 4125 (2008).
[24]J. R. Lakowicz, *Instrumentation for Fluorescence Spectroscopy* (Springer, US, 1999).
[25]K. D. Machado, A. S. Dubiel, E. Deflon, I. M. Kostrzepa, S. F. Stolf, D. F. Sanchez, and P. Jóvári, Solid State Commun. **150**, 1359 (2010).
[26]F. Kadijk and F. Jellinek, J. Less-Common Met. **23**, 437 (1971).
[27]D. B. Shinde and V. K. Pillai, Chem.-Eur. J. **18**, 12522 (2012).
[28]V. Štengl and J. Henych, Nanoscale **5**, 3387 (2013).
[29]S. K. Lai, C. M. Luk, L. Tang, K. S. Teng, and S. P. Lau, Nanoscale **7**, 5338 (2015).
[30]Y. P. Sun, B. Zhou, Y. Lin, W. Wang, K. A. S. Fernando, P. Pathak, M. J. Meziani, B. A. Harruff, X. Wang, H. Wang, P. G. Luo, H. Yang, M. E. Kose, B. Chen, L. M. Veca, and S. Y. Xie, J. Am. Chem. Soc. **128**, 7756 (2006).
[31]D. Pan, J. Zhang, Z. Li, and M. Wu, Adv. Mater. **22**, 734 (2010).
[32]L. Tang, R. Ji, X. Cao, J. Lin, H. Jiang, X. Li, K. S. Teng, C. M. Luk, S. Zeng, J. Hao, and S. P. Lau, ACS Nano **6**, 5102 (2012).